

# Carbonylation Contributes to SERCA2a Activity Loss and Diastolic Dysfunction in a Rat Model of Type 1 Diabetes

Chun Hong Shao,<sup>1</sup> Haley L. Capek,<sup>2</sup> Kaushik P. Patel,<sup>3</sup> Mu Wang,<sup>4</sup> Kang Tang,<sup>3</sup> Cyrus DeSouza,<sup>5</sup> Ryoji Nagai,<sup>6</sup> William Mayhan,<sup>3</sup> Muthu Periasamy,<sup>7</sup> and Keshore R. Bidasee<sup>1,8,9</sup>

**OBJECTIVE**—Approximately 25% of children and adolescents with type 1 diabetes will develop diastolic dysfunction. This defect, which is characterized by an increase in time to cardiac relaxation, results in part from a reduction in the activity of the sarco(endo)plasmic reticulum  $\text{Ca}^{2+}$ -ATPase (SERCA2a), the ATP-driven pump that translocates  $\text{Ca}^{2+}$  from the cytoplasm to the lumen of the sarcoplasmic reticulum. To date, mechanisms responsible for SERCA2a activity loss remain incompletely characterized.

**RESEARCH DESIGN AND METHODS**—The streptozotocin (STZ)-induced murine model of type 1 diabetes, in combination with echocardiography, high-speed video detection, confocal microscopy, ATPase and  $\text{Ca}^{2+}$  uptake assays, Western blots, mass spectrometry, and site-directed mutagenesis, were used to assess whether modification by reactive carbonyl species (RCS) contributes to SERCA2a activity loss.

**RESULTS**—After 6–7 weeks of diabetes, cardiac and myocyte relaxation times were prolonged. Total ventricular SERCA2a protein remained unchanged, but its ability to hydrolyze ATP and transport  $\text{Ca}^{2+}$  was significantly reduced. Western blots and mass spectroscopic analyses revealed carbonyl adducts on select basic residues of SERCA2a. Mutating affected residues to mimic physico-chemical changes induced on them by RCS reduced SERCA2a activity. Preincubating with the RCS, methylglyoxal (MGO) likewise reduced SERCA2a activity. Mutating an impacted residue to chemically inert glutamine did not alter SERCA2a activity, but it blunted MGO's effect. Treating STZ-induced diabetic animals with the RCS scavenger, pyridoxamine, blunted SERCA2a activity loss and minimized diastolic dysfunction.

**CONCLUSIONS**—These data identify carbonylation as a novel mechanism that contributes to SERCA2a activity loss and diastolic dysfunction during type 1 diabetes. *Diabetes* 60:947–959, 2011

**M**ore than 12 million children and adolescents worldwide have type 1 diabetes (1). In the U.S., 1.2 million children have type 1 diabetes, and ~30,000 new cases are diagnosed every year (2). There is no known way to prevent type 1 diabetes, and exogenous insulin is needed to lower/regulate blood glucose levels on a daily basis. Individuals with type 1 diabetes who are unable to tightly regulate their blood glucose levels before and after meals also develop cardiovascular diseases, including heart failure, at rates 3–5 times higher than that of the general population. To date, the pathogenesis of this diabetic cardiomyopathy (DC) remains incompletely defined, and, as a result, therapeutic strategies to prevent and/or slow its progression also remain limited.

One of the earliest clinical signs that DC is developing in individuals with type 1 diabetes is that their hearts take longer to relax between contractions (3,4). Although this diastolic dysfunction is benign at rest, a sudden tachycardia can precipitate arrhythmias, some of which are fatal. An example of the latter is the devastating dead-in-bed syndrome that is triggered by nocturnal hypoglycemia-induced tachycardia in ~6% of young type 1 diabetic patients (5).

Cardiac relaxation occurs in two sequential phases: an early active phase that is initiated principally by the action of sarco(endo)plasmic reticulum  $\text{Ca}^{2+}$ -ATPase (SERCA2a) to return the evoked rise in cytoplasmic  $\text{Ca}^{2+}$  to basal levels and a later passive phase that is dependent on the distensibility of the extracellular matrix (4). Using animal models, several investigators have found reduced SERCA2a activity during type 1 diabetes (6,7). Despite its central role in diastole, mechanisms underlying SERCA2a activity loss during type 1 diabetes remain incompletely defined. General explanations include a reduction in the expression arising from increased O-GluNAcylation (O-linked N-acetylglucosamine) of its transcription factor Sp1, thyroid hormone reductions, and from an increased association of its intrinsic inhibitor protein, phospholamban (PLN) (8–12). However, several laboratories, including ours, have found only minimal changes in expression levels of SERCA2a, PLN, and/or the phosphorylation status of PLN, especially during the early stages of the syndrome or with less severe experimental diabetes (i.e., blood glucose levels  $\leq 20$  mmol) (13–17). Therefore, we rationalize that uncharacterized mechanisms are at play that reduce SERCA2a activity during early type 1 diabetes.

It has been known for some time that reactive carbonyl species (RCS) are elevated in the serum and urine of patients with type 1 diabetes as a result of increased glucose and fatty acid oxidation, increased degradation of ketotic products, and increased triose pathway flux (18–20). Expression of vascular adhesion protein (VAP)-1/semicarbazide-sensitive amine oxidase (SSAO), an enzyme

From the <sup>1</sup>Department of Pharmacology and Experimental Neuroscience, University of Nebraska Medical Center, Omaha, Nebraska; the <sup>2</sup>Eppley Institute for Research in Cancer and Allied Diseases, University of Nebraska Medical Center, Omaha, Nebraska; the <sup>3</sup>Department of Cellular and Integrative Physiology, University of Nebraska Medical Center, Omaha, Nebraska; the <sup>4</sup>Department of Biochemistry and Molecular Biology, Indiana University School of Medicine, Indianapolis, Indiana; the <sup>5</sup>Department of Internal Medicine, Section of Diabetes, Endocrinology and Metabolism, University of Nebraska Medical Center, Omaha, Nebraska; the <sup>6</sup>Department of Food and Nutrition, Laboratory of Nutritional Science and Biochemistry, Japan Women's University, Tokyo, Japan; the <sup>7</sup>Department of Physiology and Cell Biology, Ohio State University Medical Center, Columbus, Ohio; the <sup>8</sup>Department of Environmental, Occupational, and Agricultural Health, University of Nebraska Medical Center, Omaha, Nebraska; and the <sup>9</sup>Nebraska Center for Redox Biology, Lincoln, Nebraska.

Corresponding author: Keshore R. Bidasee, kbidasee@unmc.edu.

Received 27 August 2010 and accepted 10 December 2010.

DOI: 10.2337/db10-1145

© 2011 by the American Diabetes Association. Readers may use this article as long as the work is properly cited, the use is educational and not for profit, and the work is not altered. See <http://creativecommons.org/licenses/by-nc-nd/3.0/> for details.

that synthesizes the potent RCS methylglyoxal, also was found to be upregulated as early as 1 week after the onset of diabetes (21). When in excess, RCS reacts with exposed arginine, lysine, and histidine residues on proteins to form carbonyl adducts by a process referred to as carbonylation (22,23). In an earlier study (24), we found elevated levels of carbonyl adducts on select basic residues of SERCA2a isolated from the hearts of streptozotocin (STZ)-induced diabetic rats. However, it was not clear whether these adducts were functionally important or an epiphenomenon of the diabetes. Therefore, the purpose of the current study was to ascertain whether carbonyl adducts formed on SERCA2a during diabetes impair its ability to transport  $\text{Ca}^{2+}$ .

## RESEARCH DESIGN AND METHODS

**Antibodies and chemicals.** SERCA2a and PLN antibodies were obtained from Thermo Fisher Scientific (Boulder, CO) and Millipore (Rochester, NY), argpyrimidine antibodies were obtained from JaiCA (Zhizuoka, Japan), and VAP-1 (H-43), actin ( $^{11}\text{C}$ ), and all secondary antibodies were purchased from Santa Cruz Biotechnology (Santa Cruz, CA). Advanced glycation end products (AGEs), 3-deoxyglycosone/imidazolone, carboxymethyllysine (CML), carboxyethyllysine, pentosidine, and pyralline were provided by Dr. Royji Nagai. SSAO was assayed using SSAO assay kits (Cell Technology, Mountain View, CA). Insulin pellets were obtained from LinShin Canada (Scarborough, Canada). Other reagents and buffers used were of the highest grade commercially available.

**Induction and verification of experimental type 1 diabetes.** Animals used in the study were approved by the institutional animal care and use committee of the University of Nebraska Medical Center and adhered to American Physiological Society's guiding principles for animal research (25). Forty-eight male SD rats were injected with freshly prepared STZ in cold 0.1 mol/L citrate buffer, pH = 4.5 (45 mg/kg i.v., 0.2 mL). Thirty-two other rats also were injected with a similar volume of citrate buffer only. Animals of similar weights and disease status were housed at 22°C with fixed 12-h light/12-h dark cycles with 30–40% relative humidity. Laboratory standard diet and tap water were given ad libitum.

**Treatment of diabetic animals.** Two weeks after the STZ injection, STZ-induced diabetic rats were randomly divided into three groups. One group was treated with the RCS scavenger, pyridoxamine (PyD;  $1.6 \text{ g} \cdot \text{kg}^{-1} \cdot \text{day}^{-1}$ ), via drinking water for 4–5 weeks and were labeled the PyD-D group (26). A second group of STZ-induced diabetic animals was treated with insulin (0.5 mm × 5 mm insulin pellet inserted subcutaneously) for 2 weeks to attain a euglycemic state (Ins-D group), starting 4–5 weeks after STZ injection. The third group of diabetic animals remained untreated (D group). Control animals also were divided into two groups: one group was treated with PyD ( $2.0 \text{ g} \cdot \text{kg}^{-1} \cdot \text{day}^{-1}$  because they drank one-third less water) (PyD-C group) (27) for 4–5 weeks, starting 2 weeks after the citrate buffer injection, whereas the other group remained untreated (C group).

### Establishing diastolic dysfunction

**Pulse-wave echocardiography.** At the end of the protocol, rats were anesthetized with acepromazine/ketamine (0.3 mL of 2:5 mixture), secured with tape in the supine position on a heated (37°C) pad, and maximal early (E) and late (A) diastolic transmitral flow velocities were measured using a Vevo 770 High Resolution In Vivo Micro Imaging System with a color flow-guided, pulsed-wave Doppler probe (716, 17.6-MHz; VisualSonics, Toronto, Canada).

**In vivo hemodynamics.** Basal and isoproterenol-induced heart rates and rates of left-ventricular pressure decline ( $-\text{dP}/\text{dt}$ ) were evaluated as described earlier (28).

**Myocytes isolation.** Ventricular myocytes were isolated from rat hearts, as described previously, using retrograde collagenase perfusion (17,28).

### Myocyte function

**Evoked  $\text{Ca}^{2+}$  transients.** Evoked  $\text{Ca}^{2+}$  transients were measured using the method described earlier (17).  $\text{Ca}^{2+}$  transients were recorded at 0.5 Hz (10 V for 10 ms) and 2.0 Hz.

**Contractile kinetics.** Contraction also was measured as described earlier (17), and contraction kinetics were measured at 0.5 Hz (10 V for 10 ms) and at 2.0 Hz.

**Sarcoplasmic reticulum  $\text{Ca}^{2+}$  load.** Myocytes were loaded with Fura-2 AM in DMEM-F12 medium containing 1.2 mmol/L  $\text{Ca}^{2+}$ , and sarcoplasmic reticulum (SR)  $\text{Ca}^{2+}$  load was assessed as described earlier (17).

**Steady-state levels of SERCA2a, PLN, and VAP-1.** Membrane vesicles were prepared from ventricular tissues of hearts from C, D, Ins-D, PyD-C, and PyD-D rats as described earlier (17,24). Western blot analyses were used to determine steady-state SERCA2a, PLN, VAP-1 (the enzyme that synthesizes

methylglyoxal [MGO]), and glyoxalase-1 (the enzyme that degrades MGO) levels using 10  $\mu\text{g}$  vesicular proteins as described earlier (17,24,28).

### Determination of carbonyl adducts

**Western blots.** Western blots using 80  $\mu\text{g}$  vesicular proteins, 1:500–1,000 primary antibodies, and 1:5,000 secondary antibodies were used to determine relative amounts of AGEs, argpyrimidine (methylglyoxal), CML, carboxyethyllysine, 3-deoxyglycosone/imidazolone, pentosidine, and pyralline antibodies on SERCA2a.

**Mass spectrometry.** SERCA2a was immunoprecipitated from membrane vesicles using a commercially available polyclonal SERCA2a antibody, as per the manufacturer's instructions (Affinity BioReagents, Boulder, CO). Immunoprecipitated SERCA2a was then purified from SDS-PAGE and digested with trypsin, desalted, and separated into two aliquots. One aliquot was subjected to matrix-assisted laser desorption/ionization–time-of-flight (MALDI-TOF) mass spectrometry (24). The second aliquot was used to determine the amino acid sequence of modified peptides using tandem mass spectrometry using nano-flow capillary liquid chromatography coupled with quadruple time-of-flight mass spectrometry (Micromass, Manchester, U.K.).

**Determination of MGO levels in ventricular tissue.** MGO levels were assessed in left-ventricular tissue using the high-performance liquid chromatographic procedure described by Thornalley et al. (29), except that 2-methylquinoxaline was used as the internal standard.

**Site-directed mutagenesis.** Four residues on SERCA2a were investigated in this study (R164, K476, K481, and R636) (see Fig. 1) because they were found to be carbonylated in this and our previous study (24). Residues were mutated singly and in combination to glycines to determine the impact of charge neutralization, to tyrosines and tryptophans to assess the impact of charge neutralization and increase in bulk (analogous to argpyrimidine and pyralline adducts), and to glutamic acids to assess the impact of charge inversion (analogous to CML or CML adducts) using QuikChange mutagenesis kits (Stratagene, La Jolla, CA) with oligo primers. Residues also were mutated to glutamines to blunt formation of MGO adducts. After mutations, plasmids were transformed into competent HB101 cells, amplified in liquid cultures, and purified using plasmid Maxi Prep (Qiagen, Valencia, CA), and mutations were confirmed using DNA sequencing. cDNA encoding human SERCA2a was provided by Dr. David McLennan (University of Toronto).

**Expression of recombinant SERCA2 protein.** Wild-type or mutant SERCA2a cDNA (10–15  $\mu\text{g}$ ) was transfected into human embryonic kidney (HEK)-293T cells (30–40% confluency) using  $\text{Ca}^{2+}$ -phosphate and grown in Petri dishes (100 mm) for 36–44 h. After this time, cells were harvested, sonicated ( $4 \times 6 \text{ s}$ ) in buffer (0.25 mol/L sucrose, 10 mmol/L histidine, pH 7.3) and a protease inhibitor mix (1 mmol/L benzamide, 2  $\mu\text{g}/\text{mL}$  leupeptin, 2  $\mu\text{g}/\text{mL}$  pepstatin A, 2  $\mu\text{g}/\text{mL}$  aprotinin, and 0.5 mmol/L phenylmethylsulfonyl fluoride) and centrifuged at 13,000 rpm for 3 min. Supernatants were collected, and relative SERCA2a content was determined using serial-dilution Western blots. HEK-293T cells were for expression and chosen because they express low levels of endogenous SERCA2a and do not express PLN.

### SERCA2 activity

**$\text{Ca}^{2+}$  uptake assays (steps 1–6 of the post-Elbers cycle [ $E_1 \rightarrow E_2$ ]).** Membrane vesicles were resuspended in 1 mL buffer (30 mmol/L Tris-HCl, pH 7.0; 100 mmol/L KCl; 5 mmol/L Na $_2\text{S}_2\text{O}_8$ ; 5 mmol/L MgCl $_2$ ; 0.15 mmol/L EGTA; 0.12 mmol/L CaCl $_2$ ; 1  $\mu\text{Ci}$   $^{45}\text{Ca}^{2+}$ ; and 10 mmol/L potassium oxalate) and were divided into  $2 \times 500\text{-}\mu\text{L}$  aliquots. One aliquot was incubated with a SERCA2a inhibitor cocktail (10  $\mu\text{mol}/\text{L}$  thapsigargin, 100  $\mu\text{mol}/\text{L}$  ammonium molybdate, and 0.05  $\mu\text{g}$  bafilomycin) and the other remained untreated.  $\text{Ca}^{2+}$  uptake assays were conducted as described by Andersen (30,31) using Na $_2$ ATP to initiate uptake. In assays involving rat heart membrane vesicles, 50  $\mu\text{mol}/\text{L}$  ryanodine was added to the incubation media for 10 min to inhibit or close the ryanodine receptor  $\text{Ca}^{2+}$  release channel.

**$\text{Ca}^{2+}$ -ATPase activity (steps 1–3 of the post-Elbers cycle).** Wild-type and mutant SERCA2a (equivalent amounts of proteins) were incubated in 500  $\mu\text{L}$  buffer (10 mmol/L HEPES, pH 7.3; 0.1 mol/L KCl; 5 mmol/L Mg $^{2+}$ ; 100  $\mu\text{mol}/\text{L}$  Ca $^{2+}$ ; 100  $\mu\text{mol}/\text{L}$  EGTA; and 2.5 mmol/L Na $_2$ -ATP) and incubated for 20 min at 37°C in the presence and absence of the  $\text{Ca}^{2+}$  ionophore, A23187 (2  $\mu\text{g}/\text{mL}$ ) (30,31). After this time, reactions were stopped and the inorganic phosphate generated from ATP hydrolysis was assessed using the malachite green colorimetric assay described previously (28).

**Statistical analysis.** Differences among values from each of the five groups (groups C, D, Ins-D, PyD-C, and PyD-D) were evaluated with ANOVA using Prism GraphPad. Data shown are means  $\pm$  SE. Results were considered significantly different if  $P < 0.05$  (95% CI).

## RESULTS

**Animal characteristics and confirmation of diastolic dysfunction.** The general characteristics of the animals used in this study are listed in Table 1. After 6–7 weeks of

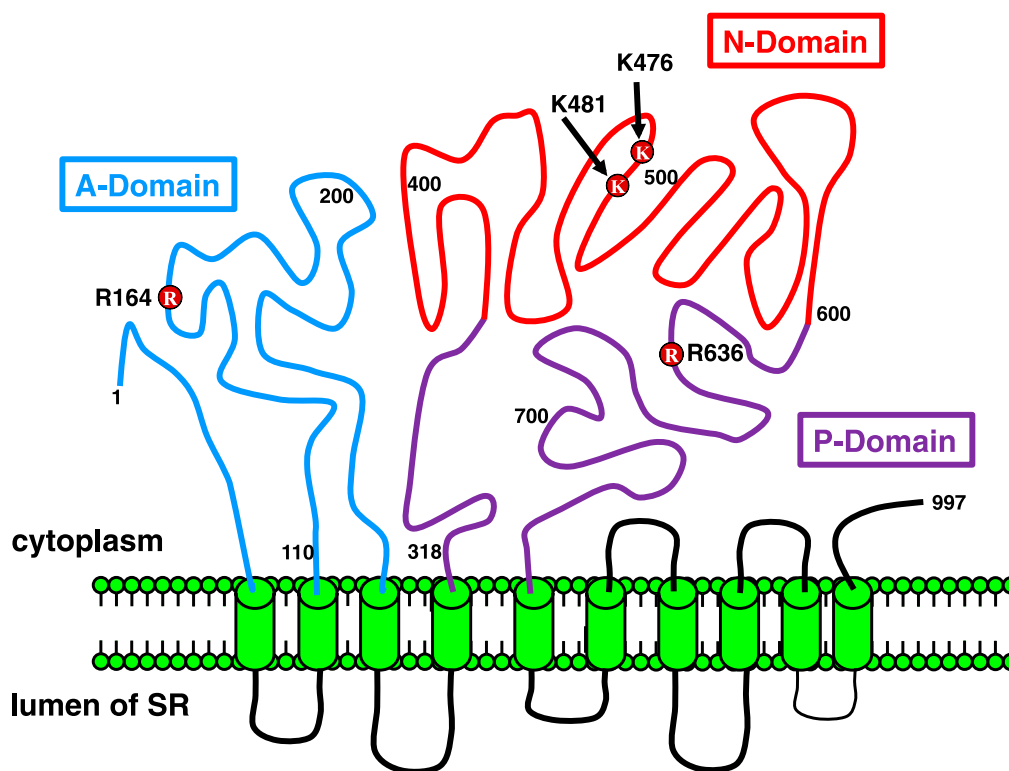


FIG. 1. Schematic showing the locations of carbonyl adducts found on SERCA2a. The structure of SERCA2a was adapted from Dode et al. (36).

diabetes, echocardiographic analyses showed characteristic reductions in early atrial-phase left-ventricular filling velocity (E) and E-to-A ratio (Fig. 2A). In vivo hemodynamics also showed a parallel increase in time to 50% relaxation ( $T_{50}$ ) (Fig. 2B). Two weeks of insulin therapy initiated 4–5 weeks after the onset of diabetes blunted decreases in blood flow velocity during diastolic filling and the E-to-A ratio (Fig. 2B) and  $T_{50}$  (Fig. 2B), establishing that diastolic dysfunction was not a result of STZ toxicity, per se, but rather diabetes.

**Diabetes slows myocyte  $\text{Ca}^{2+}$  transient decay and myocyte relaxation.** Figure 3A, *left side*, shows characteristic prolongation in myocyte  $\text{Ca}^{2+}$  transient decay time induced by diabetes at a low stimulation frequency (0.5 Hz).

Rate and amplitude of  $\text{Ca}^{2+}$  release also were reduced (Table 1, *left*) probably because of the reduced SR  $\text{Ca}^{2+}$  load (17). Mean data from >50 cells from three rats per group are shown in Table 1. Parallel reductions in contraction and relaxation velocities as well as myocyte shortening also were seen at 0.5 Hz (Fig. 3A, *right side*). Mean data are shown in Table 1, *right*.

At the higher 2-Hz stimulation, ~9% of diabetic myocytes (11 of 120) exhibited  $\text{Ca}^{2+}$  alternans (Fig. 3B, *second panel*, red line). In six of these 11 diabetic myocytes, the defect in  $\text{Ca}^{2+}$  reuptake was limited to a small segment of the scanned region (~15  $\mu\text{mol/L}$ ) (Fig. 3B, *second panel*, white arrows). Treating diabetic animals with insulin blunted the prolongation in  $\text{Ca}^{2+}$  transient decay time (Table 2). At the

TABLE 1  
General characteristics of animals

Parameter	Control (C)	STZ-induced diabetic (D)	Insulin-treated STZ-induced diabetic (Ins-D)	PyD-treated control (PyD-C)	PyD-treated STZ-induced diabetic (PyD-D)
<i>n</i>	16	16	16	15	16
Body mass (g)	370.0 ± 13.3	290.1 ± 17.3*	324.0 ± 7.5	397.6 ± 12.9	273.5 ± 15.6
Glycosylated hemoglobin (%)	4.1 ± 0.1	7.2 ± 0.1*	4.7 ± 0.2	4.2 ± 0.2	7.6 ± 0.3
Blood glucose (mmol)	5.0 ± 0.5	21.1 ± 1.4*	8.1 ± 2.1	4.9 ± 1.1	20.1 ± 1.6
Serum insulin (ng/mL)	1.02 ± 0.21	0.31 ± 0.03*	0.91 ± 0.02	1.10 ± 0.07	0.28 ± 0.04
Serum SSAO activity (units · mL <sup>-1</sup> · min <sup>-1</sup> )	0.32 ± 0.02	0.56 ± 0.03*	0.35 ± 0.06	0.22 ± 0.01	0.39 ± 0.02†
Serum T3 (ng/dL)	218.9 ± 13.1	171.8 ± 17.4*	ND	209.7 ± 20.4	174.8 ± 10.4

Data are means ± SE ( $n \geq 15$ ). \*Significantly different from control rats ( $P < 0.05$ ). †Significantly different from STZ-induced diabetic rats ( $P < 0.05$ ). ND, not done.

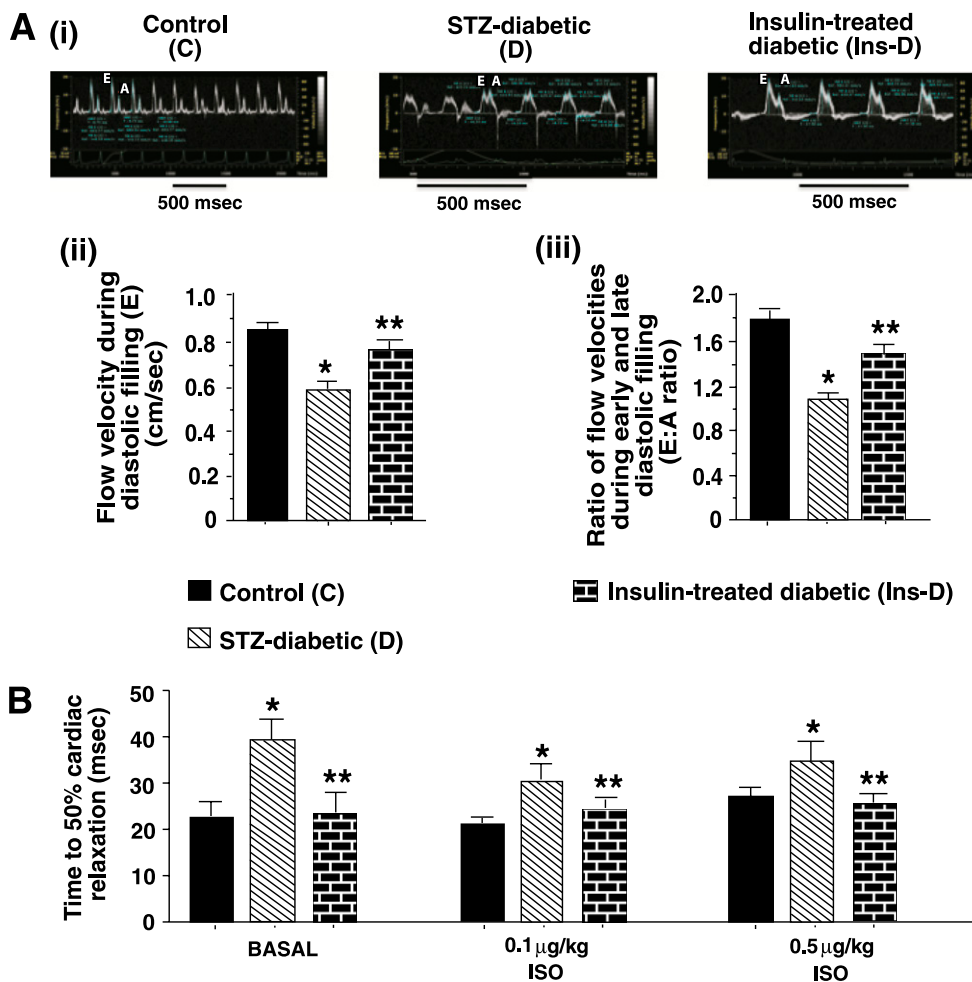


**FIG. 2. A, upper panel:** Representative pulse-wave echocardiograms of hearts from control (C), STZ-induced diabetic (D), and insulin-treated STZ-induced diabetic (Ins-D) rats. After securing the rats with tape in the supine position on a heated (37°C) pad, maximal early (E) and late (A) diastolic transmitral flow velocities were measured using a color flow-guided, pulsed-wave Doppler probe (716, 17.6 MHz). Values in the lower panels are means  $\pm$  SE ( $n \geq 8$ ). **B:** Mean time to 50% relaxation obtained from in vivo hemodynamic studies of control (C), STZ-induced diabetic (D), and insulin-treated STZ-induced diabetic rats before and after isoproterenol stimulation. Values are means  $\pm$  SE ( $n \geq 8$ ). \*Significantly different from control rats ( $P < 0.05$ ). \*\*Significantly different from STZ-induced diabetic rats ( $P < 0.05$ ). (A high-quality color representation of this figure is available in the online issue.)

2-Hz stimulation, 10 of 123 diabetic myocytes also exhibited contraction alternans (Fig. 3B, second panel, red line), which was likely the consequence of  $Ca^{2+}$  alternans. Contraction kinetics of myocytes from euglycemic animals were similar to that of control animals (Table 2).

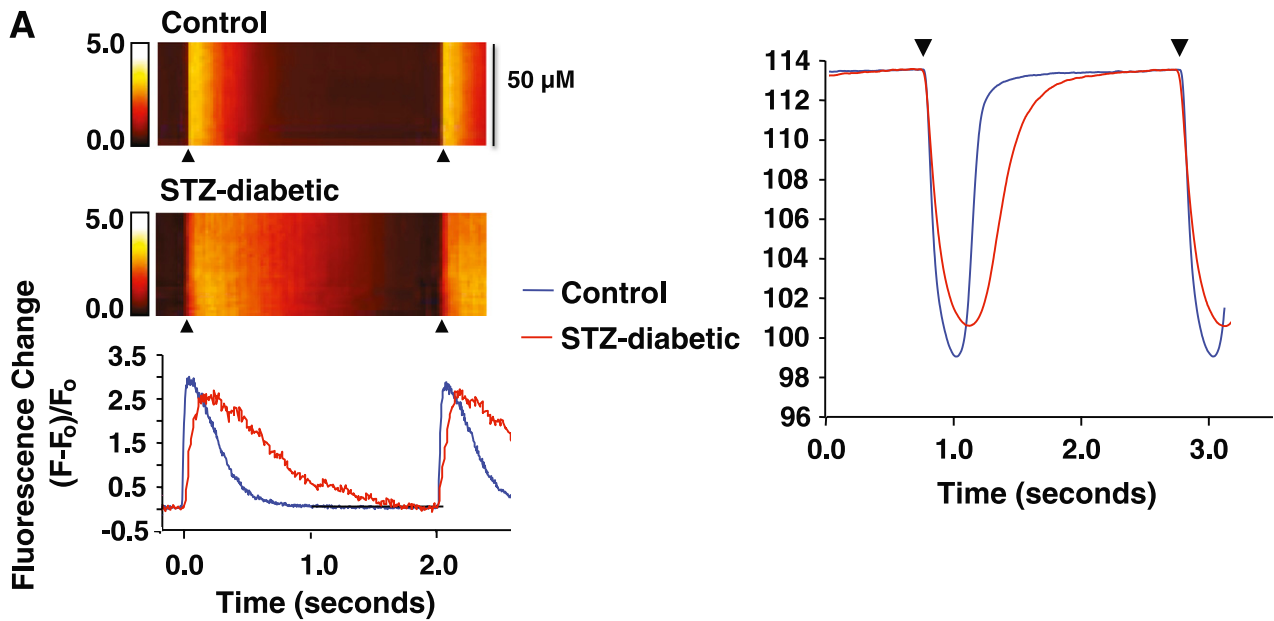
**SERCA2a activity is reduced independent of protein levels.** Minimal change in steady-state SERCA2a and monomeric PLN proteins were found in rat ventricular tissues after 6–7 weeks of diabetes (Fig. 4A). There was slight decrease ( $<10\%$ ,  $P > 0.05$ ) in pentameric (phospho-Ser16) PLN. The ability of SERCA2a to hydrolyze ATP and transport  $Ca^{2+}$  ( $E_1 \rightarrow E_2$ ) were  $30.1 \pm 6.3\%$  and  $35.2 \pm 6.4\%$  lower in diabetic animals (Figs. 4B and C). Treating diabetic animals with insulin did not alter steady-state SERCA2a or PLN proteins, but it blunted SERCA2a activity loss.

**Assessment of argpyrimidine and other carbonyl adducts on SERCA2a during diabetes.** The MGO-derived argpyrimidine adduct was threefold higher on SERCA2a from diabetic animals compared with controls (Fig. 5A, upper autoradiogram). Other adducts such as AGEs, CML, pentosidine, and pyralline also were increased 1.2- to 5-fold during diabetes (Fig. 5A). The amount of immunoreactive 3-deoxyglucosone/imidazolone and

carboxyethyllysine did not change on SERCA2a after 6–7 weeks of diabetes.

Mass spectrometry (MALDI-TOF and tandem) were then used to identify and confirm the locations of carbonyl adducts on SERCA2a. As shown in Fig. 5B, alignment of MALDI-TOF data revealed the presence of an M+1 peak at 2485.12 Da in the diabetic sample but not in control or insulin-treated SERCA2a samples. Our Perl algorithm (32) suggests that this mass could arise from a pentosidine adduct cross-linking K460 ( $_{452}MNVFDTELKGLSK_{464}$ ) in the nucleotide (N) domain and R636 ( $_{629}GTAVAIRR_{637}$ ) in the phosphorylation (P) domain. Fragmentation of the 2,485.12 Da peak afforded M+1 peaks at 950.4286, 708.3023, 607.2547, 492.2273, 347.2286, 246.0902, and M+1 peaks at 230.1132, 329.1814, 400.2190, and 513.3027, corresponding to b and y M+1 ions from MNVFDTELKGLSK and M+1 b ions from GTAVAIRR, respectively (Fig. 5C). The combination MALDI-TOF followed by tandem mass spectrometry confirmed argpyrimidine on R164, pyralline on K476 and K481, and CML adduct on R636.

**Steady-state levels of VAP-1, MGO, and glyoxalase-1 in rat heart during diabetes.** Because the argpyrimidine adduct arises from elevation in MGO, we then sought to

Ca<sup>2+</sup> transient table (UPPER-left side)

Parameter (0.5 Hz stimulation)	Control (C) (n = 53)	STZ-diabetic (D) (n=55)
Rate of Ca <sup>2+</sup> rise (f.u./sec)	39.2 ± 2.1	32.1 ± 0.8*
Peak Ca <sup>2+</sup> amplitude (f.u.)	3.2 ± 0.1	2.8 ± 0.2*
Time to peak Ca <sup>2+</sup> (msec)	70.2 ± 6.3	110.2 ± 8.6*
Rate constant of Ca <sup>2+</sup> decay (sec <sup>-1</sup> )	3.8 ± 0.3	2.1 ± 0.3*
T <sub>50</sub> decay (msec)	286.5 ± 10.1	730.1 ± 12.5*

Edge detection table (UPPER-right side)

Parameter (0.5 Hz stimulation)	Control (C) (n = 50)	STZ-diabetic (D) (n=52)
Cell length (μm)	114.5 ± 2.1	115.7 ± 1.8
Contraction velocity (μmsec <sup>-1</sup> )	148.0 ± 7.1	122.2 ± 4.0*
Percent cell shortening	12.1 ± 0.3	11.1 ± 0.3*
Relaxation velocity (μmsec <sup>-1</sup> )	101.3 ± 7.3	85.2 ± 3.5*
Time to 50% shortening (msec)	60.2 ± 5.2	70.1 ± 4.4*
Time to 50% relaxation (msec)	223.1 ± 10.2	298.1 ± 15.6*

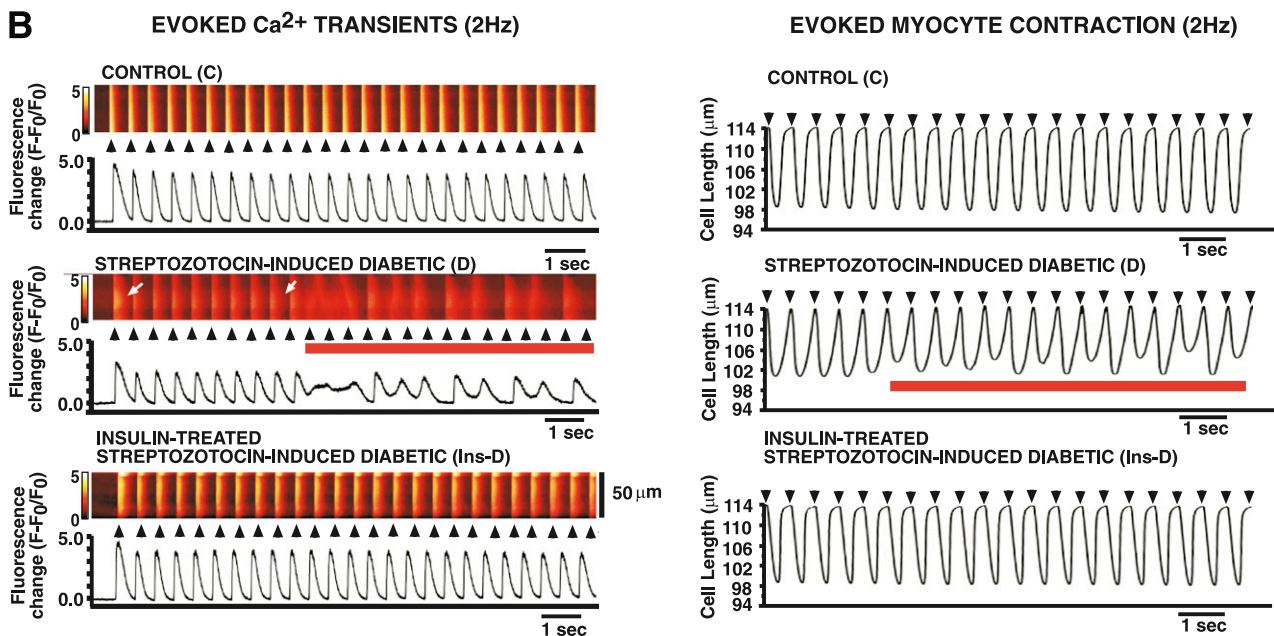


**FIG. 3. A, left side:** Representative line-scan images of a single electrically evoked global Ca<sup>2+</sup> transient and contraction kinetics (*right side*) of ventricular myocyte from control (C) and STZ-induced diabetic (D) rats. Values shown in the *lower panel* are means ± SE for  $n > 50$  cells. \*Significantly different from control rats ( $P < 0.05$ ). **B, left side:** Consecutive evoked Ca<sup>2+</sup> transients ( $\geq 20$ ) in ventricular myocytes isolated from control (C), STZ-induced diabetic (D), and insulin-treated STZ-induced diabetic (Ins-D) rat hearts stimulated at 2 Hz. **B, right side:** Consecutive evoked contractions ( $\geq 20$ ) of ventricular myocytes isolated from control (C), STZ-induced diabetic (D), and insulin-treated STZ-induced diabetic (Ins-D) rat hearts stimulated at 2 Hz. Black arrows indicate application of field stimulation (2 Hz), and red lines indicate abnormal Ca<sup>2+</sup> transients and contractions. White arrows (*left panel*) represent variation in Ca<sup>2+</sup> decay time along the scanned segment. (A high-quality digital representation of this figure is available in the online issue.)

TABLE 2

Ca<sup>2+</sup> transient parameters for myocytes from control, STZ-induced diabetic, insulin-treated STZ-induced diabetic, PyD-treated control, and PyD-treated STZ-induced diabetic rat hearts stimulated at 2 Hz

Parameter	Myocyte Ca <sup>2+</sup> transients				
	C	D	Ins-D	PyD-C	PyD-D
<i>n</i>	118	120	108	101	119
Rate of Ca <sup>2+</sup> rise (fu/s)	78.8 ± 9.4	50.4 ± 1.1*	76.4 ± 2.1†	73.6 ± 6.2	64.0 ± 2.3†
Peak Ca <sup>2+</sup> amplitude (fu)	3.9 ± 0.2	2.5 ± 0.1*	4.1 ± 0.1†	3.4 ± 0.2	3.3 ± 0.2†
T <sub>50</sub> decay (ms)	286.5 ± 10.1	730.1 ± 12.5*	320.1 ± 15.5†	229.6 ± 10.8	402.4 ± 20.1†
Parameter	Myocyte contractility				
	C	D	Ins-D	PyD-C	PyD-D
<i>n</i>	120	123	101	94	116
Cell length (μm)	111.1 ± 3.8	115.8 ± 2.8	112.1 ± 2.0	115.7 ± 4.3	114.6 ± 4.2
Contraction velocity (μm/s)	178.1 ± 7.8	110.8 ± 5.3*	139.7 ± 6.9†	174.5 ± 4.2	149.2 ± 3.1†
Percentage cell shortening	13.5 ± 0.5	10.7 ± 0.5*	11.5 ± 0.1†	11.7 ± 1.1	11.8 ± 0.2†
Relaxation velocity (μm/s)	148.8 ± 8.3	103.9 ± 5.9*	127.2 ± 5.9†	156.1 ± 6.6	132.2 ± 4.2†
Time to 50% shortening (ms)	52.6 ± 0.6	69.3 ± 1.6*	53.6 ± 0.5†	56.1 ± 1.8	59.1 ± 1.2†
Time to 50% relaxation (ms)	281.1 ± 5.5	338.9 ± 7.9*	291.0 ± 5.2†	260.3 ± 3.6	300.1 ± 6.2†

Myocyte Ca<sup>2+</sup> transients: data are means ± SE (*n* ≥ 100 cells). Myocyte contraction: Data are means ± SE (*n* ≥ 94 cells). Contractile properties of myocytes from control (C), STZ-induced diabetic (D), insulin-treated STZ-induced diabetic (Ins-D), PyD-treated control (PyD-C), and PyD-treated STZ-induced diabetic (PyD-D) rats stimulated at 2 Hz. \*Significantly different from control rats (*P* < 0.05). †Significantly different from diabetic rats (*P* < 0.05).

determine whether expression of the enzyme that synthesizes and the enzyme that degrades MGO (i.e., VAP-1 and glyoxalase-1) were altered in ventricular tissues during diabetes. Consistent with the increase in activity of its soluble form SSAO (Table 1), the steady-state level of membrane-bound VAP-1 was ~threefold higher in ventricular homogenates and myocytes from STZ-induced diabetic rats (Fig. 6A). Only the monomeric form of VAP-1 (84 kDa) was detected in these studies, probably because of denaturing conditions used to run polyacrylamide gels. Glyoxalase-1 also was increased threefold in left-ventricular myocytes during diabetes (Fig. 6B). MGO levels were twofold higher in ventricular homogenates from STZ-induced diabetic rats vs. 3.8 ± 0.5 μmol/L per 200 mg tissue in STZ-induced diabetic rats vs. 3.8 ± 0.5 μmol/L per 200 mg in controls).

**Assessing the importance of amino/azido moieties on amino acid residues of SERCA2a found to be carbonylated during diabetes.** Because SERCA2a undergoes a series of timed conformational changes to hydrolyze ATP and transport Ca<sup>2+</sup> (33), adducts like pentosidine, which cross-link intra- and interdomain residues, will likely impair the rate of conformation change and the ability of SERCA2a to translocate Ca<sup>2+</sup> from the cytoplasm to the lumen of the SR. What remains uncertain is whether non-cross-linking adducts, such as argpyrimidine, CML, and pyralline, also will do the same; if they do, are their effects on SERCA2a function residue and adduct dependent?

To date, chemical methods to insert a specific carbonyl adduct onto a specific amino acid without disrupting the tertiary structure of SERCA2a are unavailable. Because

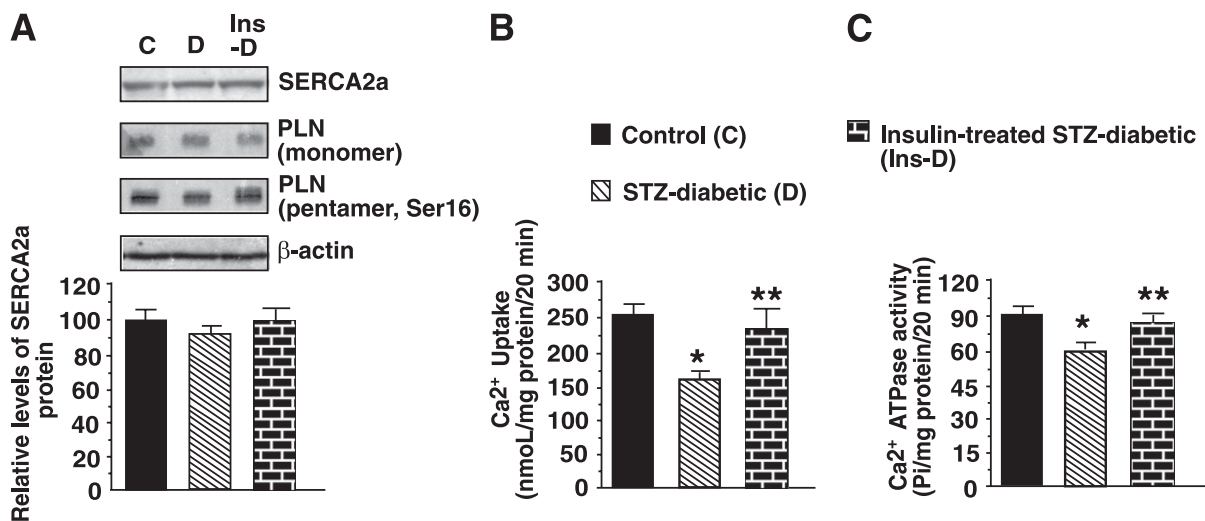
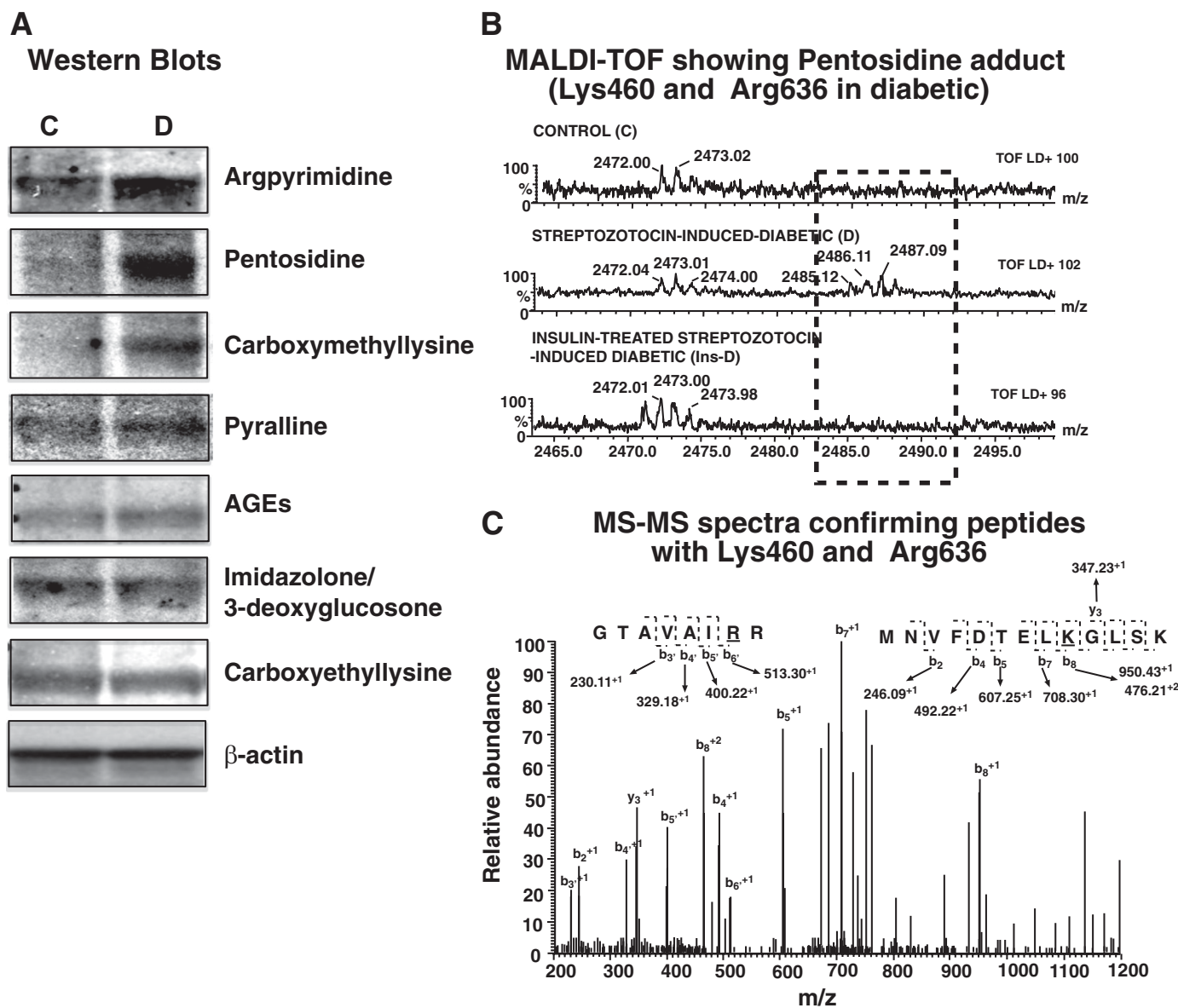


FIG. 4. A: Representative autoradiogram showing relative levels of SERCA2a, monomeric, and pentameric (Ser16) PLN protein in whole-heart homogenate from control (C), STZ-induced diabetic (D), and insulin-treated STZ-induced diabetic (Ins-D) rats. The graph below shows the relative levels of SERCA2a protein. B: The ability of SERCA2a from control (C), STZ-induced diabetic (D), and insulin-treated STZ-induced diabetic (Ins-D) rats to transport Ca<sup>2+</sup> (E1→E2). The graph shows means ± SE in *n* ≥ 7 different preparations. C: Ca<sup>2+</sup>-ATPase activity of SERCA2a from control (C), STZ-induced diabetic (D), and insulin-treated STZ-induced diabetic (Ins-D) rats. The graph shows means ± SE in *n* ≥ 5 different preparations. \*Significantly (*P* < 0.05) different from control rats. \*\*Significantly (*P* < 0.05) different from STZ-induced diabetic rats.



**FIG. 5. A:** Representative autoradiograms of carbonyl adducts on SERCA2a isolated from control (C) and STZ-induced diabetic (D) rats. Immunoblots were obtained using 75–100  $\mu\text{g}$  of membrane vesicles using argpyrimidine, AGEs, 3-deoxyglucosone/imidazolone, CML, carboxyethyllysine, pentosidine, pyralline, and actin as the primary antibodies (1:500–1,000 dilution) in Western blot assays. Data shown are consistent in all four experiments performed using different membrane preparations. **B, upper panel:** Alignment of a segment of MALDI-TOF mass spectra obtained following trypsin digestion of SERCA2a from control (C), STZ-induced diabetic (D), and insulin-treated STZ-induced diabetic (Ins-D) rats. An M+1 peak is present at 2,485.12 Da in diabetic samples but not in the others. **B, lower panel:** Tandem data corresponding to the M+1 and M+2 peaks obtained after fragmentation of peak 2,485.12 Da. Data obtained suggests that 2,485.12 Da corresponds to a pentosidine adduct between K460 ( $_{452}\text{MNVFDELKGLSK}_{464}$ ) in the nucleotide (N) domain and R636 ( $_{629}\text{GTAVAIRR}_{637}$ ) in the phosphorylation (P) domain, consistent with our PERL script prediction.

carbonylation 1) neutralizes the basic charge, 2) increases bulk, and 3) in some cases changes the free basic group to an acidic moiety, we reasoned that site-directed mutagenesis could provide insights into the role these basic amino acids are playing in the overall functioning of SERCA2a and, by extension, the impact physio-chemical changes induced on them by carbonylation will have on the ability of SERCA2a to transport  $\text{Ca}^{2+}$ . Three of four residues investigated in this study (K476 and K481 within the N domain and R636 within the P domain) are exposed to the aqueous medium, whereas the other, R164, is located within the actuator (A domain) and away from the aqueous environment ([34], also see Fig. 1).

Neutralizing basic charges on R164 and K481 by converting them to glycines significantly reduced the ability of SERCA2a to transport  $\text{Ca}^{2+}$  at all time points, indicating that these amino groups play crucial roles in SERCA2a function (Fig. 7A and C). Neutralizing basic charges on K476 and R636 had minimal impact on the ability of SERCA2a to transport  $\text{Ca}^{2+}$  within the first 10 min (Fig. 7B and D). However, as time progressed, the activities of these mutants were reduced, suggestive of “run down.” Neutralizing the basic charge and increasing hydrophilic bulk on R164 and R636 by converting them to tyrosines significantly reduced the ability of SERCA2a to transport  $\text{Ca}^{2+}$  at all time points (Fig. 7A and D). Mutating K476 and

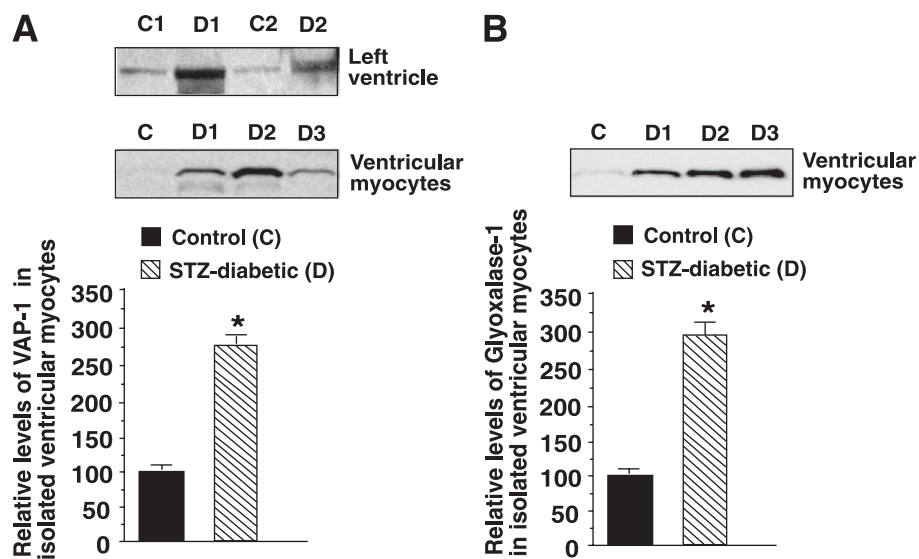


**FIG. 6.** A: Representative autoradiograms for VAP-1 in whole-heart homogenates (upper panel) and ventricular myocytes (lower panel) from control (C) and STZ-induced diabetic (D) rats. The graph below shows means  $\pm$  SE in  $n \geq 5$  different preparations. B: Representative autoradiogram for glyoxalase-1 in ventricular myocytes isolated from control (C) and STZ-induced diabetic (D) rat hearts. The graph below shows means  $\pm$  SE for  $n \geq 7$  preparations. \*Significantly ( $P < 0.05$ ) different from control.

K481 to tyrosines minimally impacted the ability of SERCA2a to transport  $\text{Ca}^{2+}$  within the first 10 min (Fig. 7B and C). However, as pumping time increased,  $\text{Ca}^{2+}$  transport rates declined. Mutating residues R164, K476, K481, and R636 to tryptophan to mimic charge neutralization and an increase in hydrophobic bulk significantly reduced the ability of SERCA2a to transport  $\text{Ca}^{2+}$  (Fig. 7A–D). Inverting the amino/azide groups on R164, K476, K481, and R636 to acidic moieties significantly reduced the ability of SERCA2a to transport  $\text{Ca}^{2+}$  (Fig. 7A–D). Neutralizing the charge, increasing bulk, or inverting the charge on two or more residues simultaneously significantly reduced the ability of SERCA2a to transport  $\text{Ca}^{2+}$  (Fig. 7E). HEK-293T cells expressed full-length wild-type and SERCA2a proteins (Fig. 7F).

To gain further insights into the mechanisms responsible for their altered  $\text{Ca}^{2+}$  transport, we also assessed the ability of SERCA2a to hydrolyze ATP. Altering the basic moiety and/or increasing bulk on K476 reduced its ability to hydrolyze ATP, in agreement with reduced  $\text{Ca}^{2+}$  uptake data (Fig. 8G). Mutating K481 to tyrosine did not affect the ability of SERCA2a to hydrolyze ATP, but the G, W, and E mutants did, in agreement with their reduced ability to transport  $\text{Ca}^{2+}$  (Fig. 7H). Neutralizing the azide moiety on R636, per se, had no impact on the ability of SERCA2a to hydrolyze ATP. However, when bulk is also added, the rate at which SERCA2a hydrolyzes ATP was reduced (Fig. 7I). Collectively, these data suggest that carbonylation at K476, K481, and R636 reduces SERCA2a activity by impairing its ability to hydrolyze ATP (steps 1–3 of the post-Elbers cycle).

**Protecting SERCA2a from the actions of methylglyoxal.** If the amino/azido groups on R164, K476, K481, and R636 are indeed important for SERCA2a activity, then preventing them from undergoing carbonylation should blunt SERCA2a activity loss.

**Mutating impacted residues to unreactive glutamines.** Glutamine mutations initially were created and confirmed on R164 and R636 because the arginine moieties on these residues are known to readily form argpyrimidine adducts with MGO. However, we were unable to express significant

quantities of R164Q and R636Q in either HEK-293T, CV-1 (simian) in origin and carrying the SV40 (COS) and Chinese hamster ovary (CHO) cells for functional studies. MGO also can form argpyrimidine adducts by utilizing adjacent amine moieties (35). Because K480 and K481 are adjacent lysines (36), this prompted us to synthesize the K481Q mutant to disrupt the adjacent amine configuration and assess whether this change can blunt the action of MGO.

When transfected into HEK-293T cells, we found that both wild-type and the K481Q mutant expressed similar amounts of full-length SERCA2a protein (Fig. 8A, upper autoradiogram). The K481Q mutant also transported  $\text{Ca}^{2+}$  (Fig. 8A, graph below) and hydrolyzed ATP (Fig. 8B) in a manner similar to that of wild-type SERCA2a, establishing that the Q mutation did not affect the normal function of SERCA2a.

Having established that the K481 mutation did not alter SERCA2a activity, we then sought to determine whether it can blunt MGO action. Preincubating wild-type SERCA2a for 20 min at 37°C with 1  $\mu\text{mol/L}$  freshly synthesized MGO (equivalent to the amount found in the serum of healthy individuals) (26) potentiated the ability of SERCA2a to transport  $\text{Ca}^{2+}$  (Fig. 8C). Preincubation with higher MGO (5–500  $\mu\text{mol/L}$ , equivalent to the amount found in the serum of diabetic patients) (26,37), dose-dependently reduced the ability of SERCA2a to transport  $\text{Ca}^{2+}$ . Interestingly, the K481Q mutant was resistant to the action of MGO (Fig. 8C), and Western blots indicate that this protection resulted directly from reduced formation of argpyrimidine (Fig. 8C, middle autoradiogram).

**Scavenging RCS in diabetic animals using PyD.** The vitamin B6 congener PyD is a potent scavenger of RCS (26), and it recently was shown to clinically reduce nephropathy in patients with type 1 and type 2 diabetes (38). We tested whether this compound also is capable of reducing carbonylation of SERCA2a and minimizing diastolic dysfunction. Treatment of STZ-induced diabetic animals with PyD did not alter blood serum glucose levels, but it blunted serum SSAO activity (Table 1). PyD treatment also blunted increases in left-ventricular pressure and cardiac relaxation times (Fig. 9A) and increases in

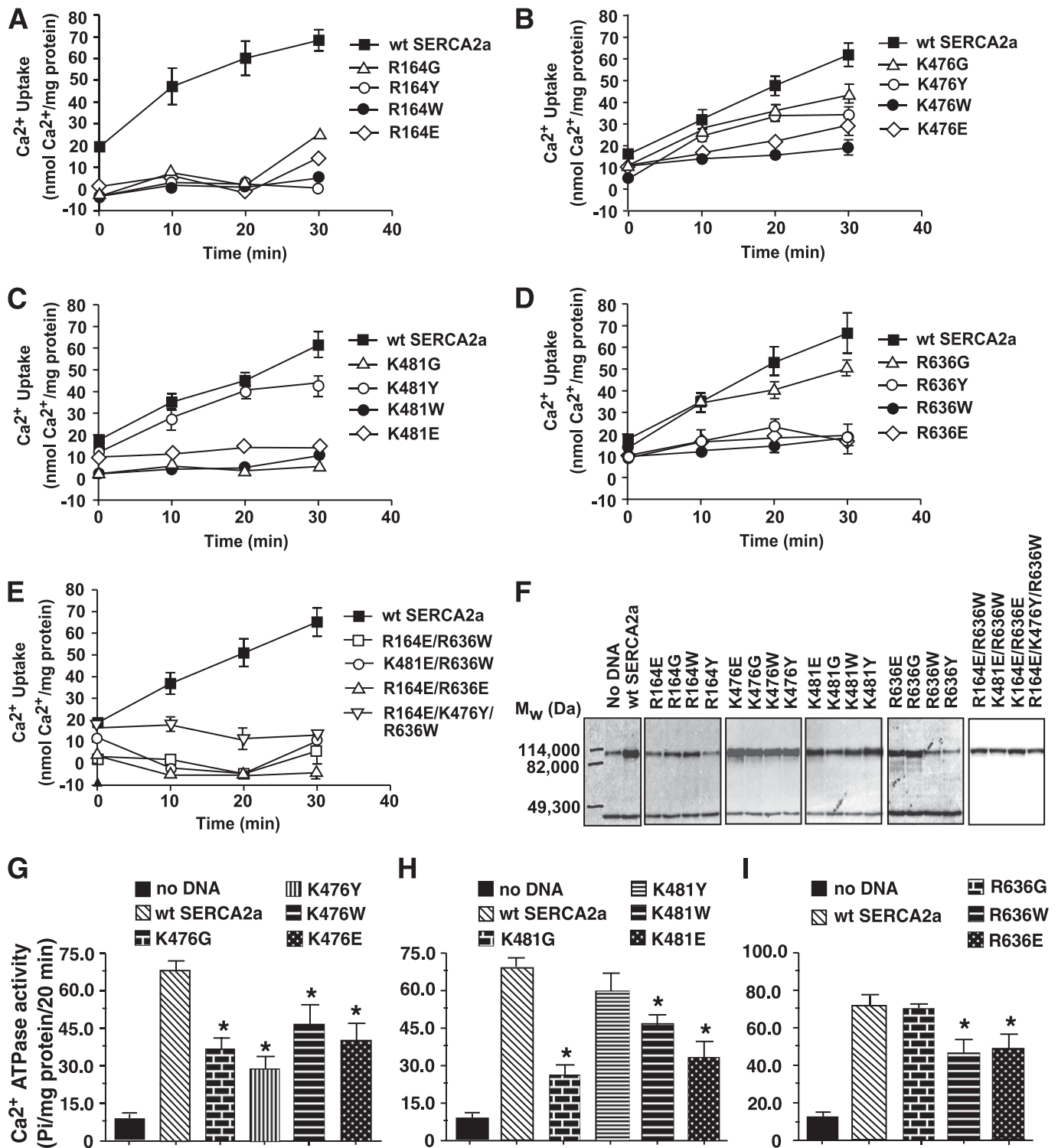


**FIG. 7.** *A–D*: The impact of a single mutation to neutralize charge (K/R→G), simultaneously neutralizing charge and increasing hydrophobic bulk (K/R→Y), simultaneously neutralizing charge and increasing hydrophilic bulk (K/R→W), and inverting charge (K/R→E) on the ability of SERCA2a to transport  $\text{Ca}^{2+}$  (E1→E2). *E*: The impact of simultaneously neutralizing charge and increasing bulk on multiple residues on the ability of SERCA2a to transport  $\text{Ca}^{2+}$  (E1→E2). *F*: Representative autoradiograms for relevant SERCA2a mutants (*upper band*), emphasizing that changes in activities observed were not a result of degradation of the SERCA2a protein. The *lower band* represents  $\beta$ -actin. *G–I*: The impact of neutralizing charge and/or increasing bulk on amino acid residues 476, 481, and 636 on the ability of SERCA2a to hydrolyze ATP (steps 2–3 of the post-Elber's cycle), respectively. Graphs are means  $\pm$  SE from  $n = 4$  experiments. \*Significantly ( $P < 0.05$ ) different from wild type.

myocyte  $\text{Ca}^{2+}$  transient decay and relaxation times (Fig. 9B; Table 2). PyD treatment also reduced expression of VAP-1 (Fig. 9C), formation of argpyrimidine and other carbonyl adducts on SERCA2a (Fig. 9D), and blunted its activity loss without altering its expression (Fig. 9E).

## DISCUSSION

In the current study, we demonstrate for the first time that by changing the charge and/or size of multiple critical basic moieties, carbonylation reduces the ability of SERCA2a to translocate  $\text{Ca}^{2+}$  from the cytoplasm to the lumen of the

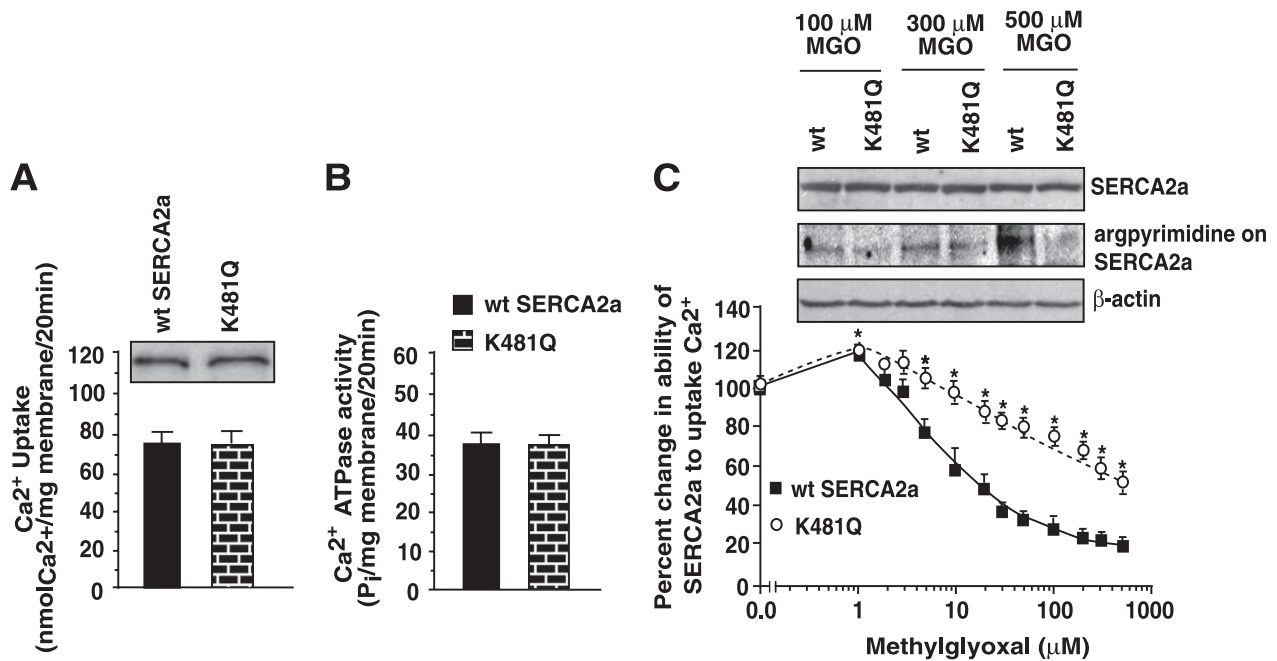


**FIG. 8. A:** Relative expression levels of wild-type SERCA2a and the K481Q SERCA2a mutant in HEK-293T cells (*upper autoradiogram*) and the ability of these proteins to transport Ca<sup>2+</sup> (*A, graph*) and hydrolyze ATP (*B*). **C:** K481Q mutation blunted the ability of MGO to reduce the ability of SERCA2a to transport Ca<sup>2+</sup> (E1→E2). For the latter, wild-type and K481Q SERCA2a proteins were incubated in buffer with varying concentrations of MGO (0–500 μmol/L) for 20 min at 37°C. At the end of this time, <sup>45</sup>Ca<sup>2+</sup> and ATP were added, and after 20 min samples were filtered. The amount of <sup>45</sup>Ca<sup>2+</sup> remaining on the filter papers was used as an index of the ability of SERCA2a to transport Ca<sup>2+</sup>. Western blot analyses also were conducted on wild-type and K481Q samples incubated with 100, 300, and 500 μmol/L MGO to determine the extent of the argpyrimidine adduct (*C, middle autoradiogram*). Western blots also were performed using SERCA2a and actin primary antibodies to ensure equivalent protein load. Values are means ± SE in *n* ≥ 3 different preparations. \*Significantly (*P* < 0.05) different from wild type.

SR. This mechanism is independent of steady-state levels of SERCA2a. In fact, in this study SERCA2a (and PLN) proteins remained essentially unchanged even though serum the T3 level was reduced by 21% during diabetes. Data from the present and our earlier study (24) also suggest that RCS does not react indiscriminately with all available basic moieties on SERCA2a. Some residues (e.g., R164, K476, K481, and R636) are more susceptible to carbonylation than others. Although the reason for this selectivity is unclear at this time, the electronic environment of the specific amino acid residue or groups of amino acids may be a contributing factor.

We also found that the amount and location of carbonylation dictates the impact it will have on SERCA2a function. With low levels of carbonylation (incubation with 1 μmol/L MGO), SERCA2a activity is actually enhanced. Adachi et al. (39) also showed that low levels of peroxynitrite oxidation resulted in gain of function of smooth-muscle SERCA. However, which residues of SERCA2a are hypersensitive to this low level of MGO remain unknown at this time. Concentrations of MGO ≥ 5 μmol/L dose-dependently reduced the ability of SERCA2a to transport Ca<sup>2+</sup>, which is consistent with the notion that carbonylation at multiple sites is needed to reduce its activity.

Neutralizing the charge and increasing hydrophilic bulk on residues exposed to the aqueous environment (K476, K481, and R636) minimally impacted the ability of SERCA2a to transport Ca<sup>2+</sup> during short-duration pumping. However, neutralizing the charge and increasing hydrophilic bulk at R164, which resides away from the aqueous environment, negatively impacted the ability of SERCA2a to transport Ca<sup>2+</sup>. Based on the work of Andersen (30,31) and Clausen et al. (40), carbonylation of A domain R164 could

be uncoupling ATP hydrolysis from calcium transport. Switching the polarity of the charge on R164, K476, K481, and R636 from basic to acidic resulted in SERCA2a activity loss, indicating that these amino/azide moieties are integral for the function of SERCA2a.

Using membrane vesicles, we found an aggregate two- to fivefold increase in carbonyl adducts on SERCA2a during diabetes. However, these data do not reveal the extent to which a specific SERCA2a molecule becomes carbonylated during diabetes and whether a few defective SERCA2a molecules are sufficient to negatively impact the overall Ca<sup>2+</sup> transient integrity. To address this question, we resorted to using confocal microscopy in the line-scan mode. In ~10% of diabetic myocytes investigated, the increase in time to Ca<sup>2+</sup> transient decay was not prolonged throughout the entire scanned region but limited to a small segment (Fig. 3B, *left side, second panel, white arrows*). We interpret this data to mean that some SERCA2a molecules are defective, whereas others are not. Interestingly, when these myocytes were stimulated at 2 Hz, Ca<sup>2+</sup> alternans were observed (Fig. 3B, *left side, second panel, red line*). In some diabetic animals we also observed cardiac ventricular fibrillation following isoproterenol injection (data not shown), but the specific causes of this remain unclear. Because Ca<sup>2+</sup> alternans is an underlying cause for ventricular arrhythmias, these data also suggest that increased carbonylation of SERCA2a may be contributing to tachycardia-induced ventricular arrhythmias during diabetes. However, it should be pointed out that defects in other SR Ca<sup>2+</sup>-cycling proteins, such as type 2 ryanodine receptor and type 2 calsequestrin also may be contributors (41,42). Based on the data from this and an earlier study (17), we speculate that perturbation in myocyte intracellular

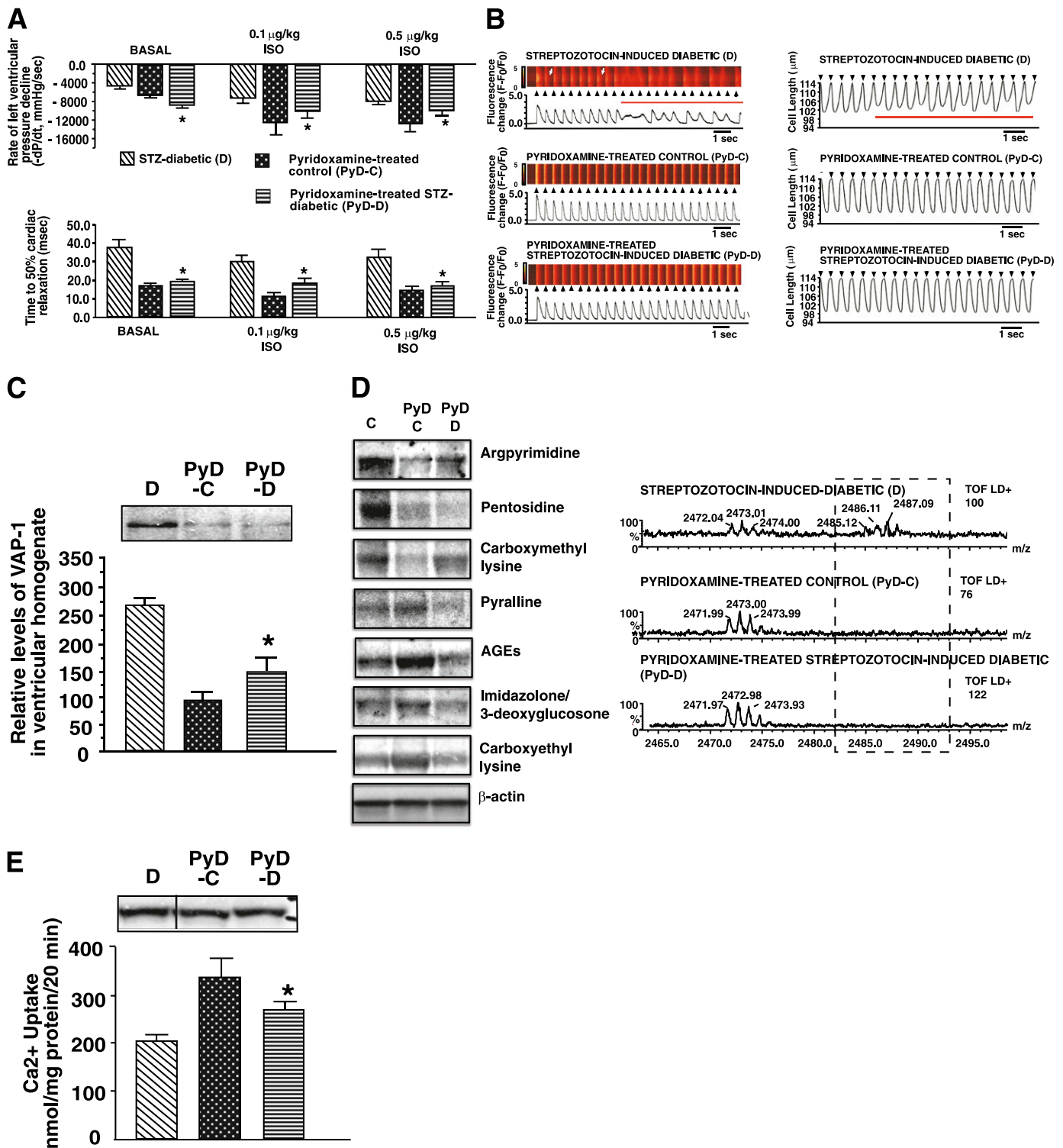


**FIG. 9.** A: Mean  $-dP/dt$  (rate of left-ventricular pressure decline) and time to 50% relaxation obtained from in vivo hemodynamic studies of STZ-induced diabetic (D), PyD-treated control (PyD-C), and PyD-treated STZ-induced diabetic (PyD-D) rats before and after isoproterenol stimulation. Values shown are means  $\pm$  SE ( $n \geq 8$ ). \*Significantly different from diabetic ( $P < 0.05$ ) rats. **B, left side:** Consecutive evoked  $Ca^{2+}$  transients ( $\geq 20$ ) in ventricular myocytes isolated from D, PyD-C, and PyD-D rat hearts stimulated at 2 Hz. **B, right side:** Consecutive contractions ( $\geq 20$ ) of ventricular myocytes isolated from D, PyD-C, and PyD-D rat hearts stimulated at 2 Hz. Black arrows indicate the application of field stimulation (2 Hz), and red lines indicate abnormal  $Ca^{2+}$  transients and contractions. White arrows (*left panel*) represent the variation in  $Ca^{2+}$  decay time along the scanned segment. **C:** Autoradiogram for relative levels of VAP-1 in hearts from D, PyD-C, and PyD-D rats. **D:** Representative autoradiograms for carbonyl adducts on SERCA2a from D, PyD-C, and PyD-D rats. Standard Western blots were used for these studies using 75–100  $\mu$ g of membrane vesicles. **D** also shows alignment of a segment of MALDI-TOF mass spectra obtained following trypsin digestion of SERCA2a from D, PyD-C, and PyD-D rats. M+1 peak at 2,485.12 Da seen in diabetic samples was not present after PyD treatment. **E:** Relative levels of SERCA2a expression in ventricular tissues from D, PyD-C, and PyD-D rats. The graph below shows the ability of SERCA2a from D, PyD-C, and PyD-D rat hearts to transport  $Ca^{2+}$ . Values shown are means  $\pm$  SE in  $n \geq 7$  different preparations. \*Significantly ( $P < 0.05$ ) different from diabetic rats. (A high-quality digital representation of this figure is available in the online issue.)

Ca<sup>2+</sup> cycling arising from defects in SERCA2a and type 2 ryanodine receptor activities may be contributing to nocturnal hypoglycemia-induced ventricular arrhythmia and the resultant dead-in-bed in young type 1 diabetic patients.

Having established that carbonyl adducts are functionally important, we then proceeded to assess whether preventing the formation of these adducts could minimize SERCA2a activity loss and, by extension, diastolic dysfunction, in vitro and in vivo. As indicated above, in vitro studies MGO (5–500 μmol/L) dose-dependently reduced the ability of SERCA2a to transport Ca<sup>2+</sup>. Mutating K481 to a glutamine to prevent MGO from forming argpyrimidine with the adjacent amino residues on K480 and K481 blunted the ability of MGO to reduce SERCA2a activity loss. We also showed that treating STZ-induced diabetic animals with the RCS scavenger PyD blunted carbonylation of SERCA2a and the diastolic dysfunction induced by diabetes. These data further strengthen the notion that carbonylation is an important mechanism underlying diabetic cardiomyopathy.

Another novel finding of the current study is that although expression of the MGO-degrading enzyme glyoxalase-1 is elevated in rat ventricular myocytes during diabetes, this increase was not sufficient to reduce formation of argpyrimidine adducts on SERCA2a. In fact, we measured and found MGO levels to be twofold higher in ventricular tissues from STZ-induced diabetic rats compared with ventricular tissues from control animals. It should also be pointed out that although this study focused on the impact of MGO on SERCA2a, MGO also is likely to react with and alter the function of other intracellular, long-lived proteins, including type 2 ryanodine receptors (43). Another interesting finding of the current study is that treatment with PyD blunted the increase in cardiac VAP-1 induced by diabetes. The latter is extremely exciting because it suggests, for the first time, that MGO and other RCS may be potentiating the expression of VAP-1/SSAO by a feed-forward mechanism.

In conclusion, this study demonstrates, for the first time, that carbonylation is an important mechanism that contributes to SERCA2a activity loss and diastolic dysfunction in a rat model of type 1 diabetes. These findings also have implications beyond that of type 1 diabetes. Elevated levels of carbonylated proteins also are found in patients with type 2 diabetes, congestive heart failure, and renal failure (44–50). Increasing expression of proteins including SERCA2a without lowering carbonyl stress is likely to only transiently blunt diastolic dysfunction during diabetes because newly expressed SERCA2a proteins will subsequently undergo carbonylation (51). We propose scavenging RCS as an adjunct therapeutic strategy for slowing diastolic dysfunction during type 1 diabetes.

#### ACKNOWLEDGMENTS

This work was supported in part by grants from the American Diabetes Association (to K.R.B.), the Edna Ittner Pediatric Research Foundation (to K.R.B.), the National Institutes of Health (NS-39751 to K.P.P., HL-090657 and AA-01128 to W.M., and HL-085061 to K.R.B.), and a grant-in-aid from the Ministry of Education, Science, Sports, and Cultures of Japan (Scientific Research Grant no. 18790619, to R.N.).

No potential conflicts of interest relevant to this article were reported.

C.H.S., H.L.C., K.P.P., M.W., K.T., C.D., W.M., and M.P. performed experiments, analyzed data, and assisted with

manuscript editing. R.N. provided critical reagents that were not commercially available. K.R.B. came up with the hypothesis, designed experiments, performed data analyses, and wrote the manuscript.

The authors thank Dr. David McLennan, University of Toronto, for human SERCA2a cDNA, and Caronda J. Moore and Matthew Dale, University of Nebraska Medical Center, Omaha, for editorial assistance.

#### REFERENCES

- International Diabetes Federation. IDF diabetes atlas [article online]. Available from <http://www.diabetesatlas.org/>. Accessed 10 August 2010
- Juvenile Diabetes Association. Fact sheet type 1 diabetes [article online]. Available from [http://www.jdrf.org/index.cfm?page\\_id=102585](http://www.jdrf.org/index.cfm?page_id=102585). Accessed 20 January 2011
- Park J-W, Ziegler AG, Janka HU, Doering W, Mehnert H. Left ventricular relaxation and filling pattern in diabetic heart muscle disease: an echocardiographic study. *Klin Wochenschr* 1988;66:773–778
- Ruddy TD, Shumak SL, Liu PP, et al. The relationship of cardiac diastolic dysfunction to concurrent hormonal and metabolic status in type I diabetes mellitus. *J Clin Endocrinol Metab* 1988;66:113–118
- Koltin D, Daneman D. Dead-in-bed syndrome: a diabetes nightmare. *Pediatr Diabetes* 2008;9:504–507
- Penpargkul S, Fein F, Sonnenblick EH, Scheuer J. Depressed cardiac sarcoplasmic reticular function from diabetic rats. *J Mol Cell Cardiol* 1981;13:303–309
- Choi KM, Zhong Y, Hoit BD, et al. Defective intracellular Ca(2+) signaling contributes to cardiomyopathy in type 1 diabetic rats. *Am J Physiol Heart Circ Physiol* 2002;283:H1398–H1408
- Clark RJ, McDonough PM, Swanson E, et al. Diabetes and the accompanying hyperglycemia impairs cardiomyocyte calcium cycling through increased nuclear O-GlcNAcylation. *J Biol Chem* 2003;278:44230–44237
- Machackova J, Barta J, Dhalla NS. Molecular defects in cardiac myofibrillar proteins due to thyroid hormone imbalance and diabetes. *Can J Physiol Pharmacol* 2005;83:1071–1091
- Kahaly GJ, Dillmann WH. Thyroid hormone action in the heart. *Endocr Rev* 2005;26:704–728
- Kim HW, Ch YS, Lee HR, Park SY, Kim YH. Diabetic alterations in cardiac sarcoplasmic reticulum Ca<sup>2+</sup>-ATPase and phospholamban protein expression. *Life Sci* 2001;70:367–379
- Rastogi S, Sentex E, Elimban V, Dhalla NS, Neticadan T. Elevated levels of protein phosphatase 1 and phosphatase 2A may contribute to cardiac dysfunction in diabetes. *Biochim Biophys Acta* 2003;1638:273–277
- Zhong Y, Ahmed S, Grupp IL, Matlib MA. Altered SR protein expression associated with contractile dysfunction in diabetic rat hearts. *Am J Physiol Heart Circ Physiol* 2001;281:H1137–H1147
- Tschöpe C, Spillmann F, Rehfeld U, et al. Improvement of defective sarcoplasmic reticulum Ca<sup>2+</sup> transport in diabetic heart of transgenic rats expressing the human kallikrein-1 gene. *FASEB J* 2004;18:1967–1969
- Zhao XY, Hu SJ, Li J, Mou Y, Chen BP, Xia Q. Decreased cardiac sarcoplasmic reticulum Ca<sup>2+</sup>-ATPase activity contributes to cardiac dysfunction in streptozotocin-induced diabetic rats. *J Physiol Biochem* 2006;62:1–8
- Ligeti L, Szczeni O, Prestia CM, et al. Altered calcium handling is an early sign of streptozotocin-induced diabetic cardiomyopathy. *Int J Mol Med* 2006;17:1035–1043
- Shao CH, Wehrens XH, Wyatt TA, et al. Exercise training during diabetes attenuates cardiac ryanodine receptor dysregulation. *J Appl Physiol* 2009;106:1280–1292
- Brownlee M, Cerami A, Vlassara H. Advanced glycosylation end products in tissue and the biochemical basis of diabetic complications. *N Engl J Med* 1988;318:1315–1321
- Brownlee M. Biochemistry and molecular cell biology of diabetic complications. *Nature* 2001;414:813–820
- Deng Y, Yu PH. Simultaneous determination of formaldehyde and methylglyoxal in urine: involvement of semicarbazide-sensitive amine oxidase-mediated deamination in diabetic complications. *J Chromatogr Sci* 1999;37:317–322
- Hayes BE, Clarke DE. Elevation of serum benzylamine oxidase activity in diabetic rats. *Proc West Pharmacol Soc* 1983;26:119–122
- Stadtman ER. Protein oxidation and aging. *Science* 1992;257:1220–1224
- Uchida K. Role of reactive aldehyde in cardiovascular diseases. *Free Radic Biol Med* 2000;28:1685–1696
- Bidasee KR, Zhang Y, Shao CH, et al. Diabetes increases formation of advanced glycation end products on Sarco(endo)plasmic reticulum Ca<sup>2+</sup>-ATPase. *Diabetes* 2004;53:463–473

25. National Research Council. Guide for the Care and Use of Laboratory Animals. Washington, DC, National Academy Press, 1996
26. Vozizyan PA, Hudson BG. Pyridoxamine: the many virtues of a maillard reaction inhibitor. *Ann N Y Acad Sci* 2005;1043:807–816
27. Nagaraj RH, Sarkar P, Mally A, Biemel KM, Lederer MO, Padayatti PS. Effect of pyridoxamine on chemical modification of proteins by carbonyls in diabetic rats: characterization of a major product from the reaction of pyridoxamine and methylglyoxal. *Arch Biochem Biophys* 2002;402:110–119
28. Shao CH, Rozanski GJ, Nagai R, et al. Carbonylation of myosin heavy chains in rat heart during diabetes. *Biochem Pharmacol* 2010;80:205–217
29. Thornalley PJ, Hooper NI, Jennings PE, et al. The human red blood cell glyoxalase system in diabetes mellitus. *Diabetes Res Clin Pract* 1989;7:115–120
30. Andersen JP. Dissection of the functional domains of the sarcoplasmic reticulum Ca(2+)-ATPase by site-directed mutagenesis. *Biosci Rep* 1995;15:243–261
31. Andersen JP. Functional consequences of alterations to amino acids at the M5S5 boundary of the Ca(2+)-ATPase of sarcoplasmic reticulum. Mutation Tyr763—>Gly uncouples ATP hydrolysis from Ca2+ transport. *J Biol Chem* 1995;270:908–914
32. Zhang Y, Cocklin RR, Bidasee KR, Wang M. Rapid determination of advanced glycation end products of proteins using MALDI-TOF-MS and PERL script peptide searching algorithm. *J Biomol Tech* 2003;14:224–230
33. Toyoshima C, Nomura H. Structural changes in the calcium pump accompanying the dissociation of calcium. *Nature* 2002;418:605–611
34. Toyoshima C, Nomura H, Tsuda T. Luminal gating mechanism revealed in calcium pump crystal structures with phosphate analogues. *Nature* 2004;432:361–368
35. Yim HS, Kang SO, Hah YC, Chock PB, Yim MB. Free radicals generated during the glycation reaction of amino acids by methylglyoxal: a model study of protein-cross-linked free radicals. *J Biol Chem* 1995;270:28228–28233
36. Dode L, Andersen JP, Leslie N, Dhitavat J, Vilsen B, Hovnanian A. Dissection of the functional differences between sarco(endo)plasmic reticulum Ca2+-ATPase (SERCA) 1 and 2 isoforms and characterization of Darier disease (SERCA2) mutants by steady-state and transient kinetic analyses. *J Biol Chem* 2003;278:47877–47889
37. Lapolla A, Flamini R, Dalla Vedova A, et al. Glyoxal and methylglyoxal levels in diabetic patients: quantitative determination by a new GC/MS method. *Clin Chem Lab Med* 2003;41:1166–1173
38. Williams ME, Bolton WK, Khalifah RG, Degenhardt TP, Schotzinger RJ, McGill JB. Effects of pyridoxamine in combined phase 2 studies of patients with type 1 and type 2 diabetes and overt nephropathy. *Am J Nephrol* 2007;27:605–614
39. Adachi T, Weisbrod RM, Pimentel DR, et al. S-Glutathiolation by peroxynitrite activates SERCA during arterial relaxation by nitric oxide. *Nat Med* 2004;10:1200–1207
40. Clausen JD, McIntosh DB, Vilsen B, Woolley DG, Andersen JP. Importance of conserved N-domain residues Thr441, Glu442, Lys515, Arg560, and Leu562 of sarcoplasmic reticulum Ca2+-ATPase for MgATP binding and subsequent catalytic steps: plasticity of the nucleotide-binding site. *J Biol Chem* 2003;278:20245–20258
41. Marks AR, Priori S, Memmi M, Kontula K, Laitinen PJ. Involvement of the cardiac ryanodine receptor/calcium release channel in catecholaminergic polymorphic ventricular tachycardia. *J Cell Physiol* 2002;190:1–6
42. Terentyev D, Viatchenko-Karpinski S, Györke I, Volpe P, Williams SC, Györke S. Calsequestrin determines the functional size and stability of cardiac intracellular calcium stores: Mechanism for hereditary arrhythmia. *Proc Natl Acad Sci USA* 2003;100:11759–11764
43. Ferrington DA, Kraivnev AG, Bigelow DJ. Altered turnover of calcium regulatory proteins of the sarcoplasmic reticulum in aged skeletal muscle. *J Biol Chem* 1998;273:5885–5891
44. Dunkel P, Gelain A, Barlocco D, et al. Semicarbazide-sensitive amine oxidase/vascular adhesion protein 1: recent developments concerning substrates and inhibitors of a promising therapeutic target. *Curr Med Chem* 2008;15:1827–1839
45. Penckofer S, Schwertz D, Florczak K. Oxidative stress and cardiovascular disease in type 2 diabetes: the role of antioxidants and pro-oxidants. *J Cardiovasc Nurs* 2002;16:68–85
46. Kilhovd BK, Berg TJ, Birkeland KI, Thorsby P, Hanssen KF. Serum levels of advanced glycation end products are increased in patients with type 2 diabetes and coronary heart disease. *Diabetes Care* 1999;22:1543–1548
47. Schalkwijk CG, Baidoshvili A, Stehouwer CD, van Hinsbergh VW, Niessen HW. Increased accumulation of the glycoxidation product Nepsilon-(carboxymethyl)lysine in hearts of diabetic patients: generation and characterisation of a monoclonal anti-CML antibody. *Biochim Biophys Acta* 2004;1636:82–89
48. Koyama Y, Takeishi Y, Arimoto T, et al. High serum level of pentosidine, an advanced glycation end product (AGE), is a risk factor of patients with heart failure. *J Card Fail* 2007;13:199–206
49. Boomsma F, van Veldhuisen DJ, de Kam PJ, et al. Plasma semicarbazide-sensitive amine oxidase is elevated in patients with congestive heart failure. *Cardiovasc Res* 1997;33:387–391
50. Miyata T, Inagi R, Kurokawa K. Diagnosis, pathogenesis, and treatment of dialysis-related amyloidosis. *Miner Electrolyte Metab* 1999;25:114–117
51. Karakikes I, Kim M, Hadri L, et al. Gene remodeling in type 2 diabetic cardiomyopathy and its phenotypic rescue with SERCA2a. *PLoS ONE* 2009;4:e6474